Examination of Flow Effects in Francis Turbine Models with Different Numbers of Rotor Blades

Selçuk KEÇEL[1], H. Güçlü YAVUZCAN[1], Adnan SÖZEN[2*]
[1]Gazi University, Faculty of Architecture, Department of Industrial Product Design
[2]Gazi University, Faculty of Technology, Department of Energy Systems Engineering

ABSTRACT

This study reviews velocity-pressure changes in spiral case, rotor and outlet pipes, force-torque values affecting the turbine rotor, vortexes in the outlet pipe, and pressure changes and vibration effects on two models with different numbers of rotor blades. The study evaluates the effect of different numbers of rotor blades on the flow and the effects on turbine components to obtain maximum turbine power. Furthermore, this study evaluates the relationship between the number of rotor blades and guide rotor blades on velocity-pressure interactions. The analysis determined the turbine rotor blade number to be 17 (Model 1) and 20 (Model 2) and the wicket gate angle was altered between 12°-48° to analyze the effects on turbine characteristics (velocity, pressure, torque, vortex, and power).

Keywords: Design of Francis Turbine, Computational Fluid Dynamics, Turbomachinery.

Farklı Rotor Kanat Sayısına Sahip Francis Türbin Modellerinde Akış Etkilerinin İncelenmesi

ÖZ

Bu çalışmada farklı rotor kanat sayılarına sahip iki model üzerinde, salyangoz, rotor ve çıkış borularındaki hız-basınç değişimleri, türbin rotoruna etkiyen kuvvet-tork değerleri, çıkış borusunda oluşan vorteksler ile basınç değişimleri ve titreşim etkileri incelenmiştir. Çalışmada maksimum türbin gücü elde edebilmek için farklı sayıya sahip rotor kanatlarının akışa olan etkisi değerlendirilmiş ve türbin bileşenlerinde meydana gelen etkiler incelenmiştir. Ayrıca rotor kanat sayıları ile yönlendirme kanat açıları arasındaki ilişki hız-basınç etkileşimleri üzerinde incelenmiştir. Yapılan analizlerde türbin rotor kanat sayısı 17 (Model-1) ve 20 (Model-2) olarak belirlenmiş ve yönlendirme kanat açısı 12o-48o aralığında değiştirilerek türbin karakteristikleri (hız, basınç, tork, verim ve güç gibi) üzerinde oluşan etkiler incelenmiştir.

Anahtar Kelimeler: Francis türbini tasarımı, Hesaplamalı Akışkanlar Dinamiği (HAD), Turbomakinalar.

1. INTRODUCTION (GİRİŞ)

Computational Fluid Dynamics (CFD) analyses have powerful design tools to display flow characteristics of hydraulic power components. Many researchers have benefited from CFD applications while analyzing rotor-stator interactions, cavitation behaviors, and performance under various loads in the computational analysis of Francis turbines.

Čarija et al. (2010) made an analysis with CFD for different discharge flows in the outlet pipe of a Francis turbine system. Fifteen rotor blades were used in the model with 20 wicket gates; vortexes in the outlet pipe were reviewed and small changes were observed in efficiency levels [1]. Ruofu et al.(2008) studied pressure distribution on the turbine rotor under seven different boundary conditions (68%-75%-85%-92%-100%-106%-113%) for partial, normal, and extreme loads with a fixed head value[2]. Choi et al. (2013) made an optimization through CFD on a 500kW horizontal axis Francis turbine

measurements and obtained improvements in efficiency up to 9.96% [3]. In the study performed by Saaed et al. (2010), different models constructed to reduce the stresses on the vanes of the turbine were investigated. In these models, components of the radial and tangential velocity as well as the strength of the vanes at different loading and flow rate values were examined. In the parametric model constructed by, the flow analysis of the exit tubes and their structural analysis were performed. In the structural analysis, total deformation and forces creating stress were visualized [4]. In another study performed by Okyay et al. (2009), Francis turbine design related with computational fluid dynamics was performed and variation in the pressure of grid structure which raised around the stay vanes and spiral was demonstrated [5]. In two study performed by Chen (2009), the stresses on wicket gate and rotating runner of a Francis turbine formed by a flow were examined by finite elements method [6]. Jain, et al. (2010) reviewed the rates of input-output powers at different flow rates in a study for efficiency estimation with the help of CFD in a horizontal axis Francis turbine. They obtained output values on two different boundary conditions (pressure

input and mass flow input) and provided recommendations to the manufacturers [7]. Pennacchi et al. (2011) developed a model to reduce vibration on turbine blades. They attempted to reduce vibration on blades with a compression mechanism on connection points of blades [8]. Zhange et al. (2012) studied cavitation behaviors of a high head Francis turbine under partial load. They developed an empirical relationship for cavitation amounts in areas close to the turbine wheel and the output pipe [9]. Bing et al. (2012) studied vibrations on the main shaft system with ANSYS software for critical rotational speeds and made certain dynamic analyses to be used as a reference in turbine design [10]. Nilsson et al. (2000) calculated velocity and pressure effectiveness at certain distances by changing angles of the output axis for Kaplan and Francis water turbine wheels [11].

This study obtained geometric values for the turbine with calculations for six different models in the literature according to data for a point with a known flow rate and head values. The turbine was designed with one of the various calculation techniques, the Kuarner method [12]. The number of wicket gates were obtained and the wheel was designed with geometric values of the turbine. The designed turbine scroll, fixed blades, wheel and outlet pipes were prepared and analyzed with the modules in CFD software.

2. FLOW SIMULATIONS (AKIŞ SİMÜLASYONLARI)

2.1. Geometric model (Geometrik Model)

To the start turbine design, a flow rate of $56.15 m^3/h$ and a head value of 100m were set as the physical parameters, the number of revolutions was $250 min^{-1}$ according to different calculation results based on these values. Moreover, while selecting the number of revolutions, the Kuarner method, which provided the closest value to $250 min^{-1}$, was selected after calculations with the methods in Table 1.

The Kuarner method was preferred considering its compliance with design criteria in terms of specific speed, flow rate, power parameters, and the statement : "*The output of Francis turbines with a specific speed of $150 min^{-1}$ to $250 min^{-1}$ is known to be better than others [12]*" in literature. Additionally, the most important point to consider while selecting the specific speed and the number of revolutions is to select "n_s" upper limit and "n" lower limit to obtain maximum power from a certain head value. It should also be noted that with more turbine revolutions, the size of turbines and plants will decline, and hydromechanical and electromechanical parts will cost less; on the other hand, the plant will be immersed deeper to resist cavitation and construction costs will increase [12,13].

Table 1. Methods for calculation of the specific rotation speed (Özgül devir sayısı hesaplama metotları)

Method	$n_s (min^{-1})$	$n_s (min^{-1})$	$n (min^{-1})$	$n (min^{-1})$
Osterien	$n_s = 3500/H_d^{0.7}$	$n_s = 142.3$	$n = n_s(H_d^{1.25})/(P^{0.5})$	$n = 172.8$
Voith	$n_s = 4140/H_d^{0.7}$	$n_s = 168.3$	$n = n_s(H_d^{1.25})/(P^{0.5})$	$n = 204.4$
Kuarner	$n_s = 5000/H_d^{0.7}$	$n_s = 203.3$	$n = n_s(H_d^{1.25})/(P^{0.5})$	$n = 246.9$
Egzozarof	$n_s = 5000/H_d^{0.75}$	$n_s = 161.7$	$n = n_s(H_d^{1.25})/(P^{0.5})$	$n = 196.4$
USA	$n_s = 2334/H_d^{0.5}$	$n_s = 236.9$	$n = n_s(H_d^{1.25})/(P^{0.5})$	$n = 287.7$
Leva	$n_s = 3470/H_d^{0.65}$	$n_s = 177.3$	$n = n_s(H_d^{1.25})/(P^{0.5})$	$n = 215.4$
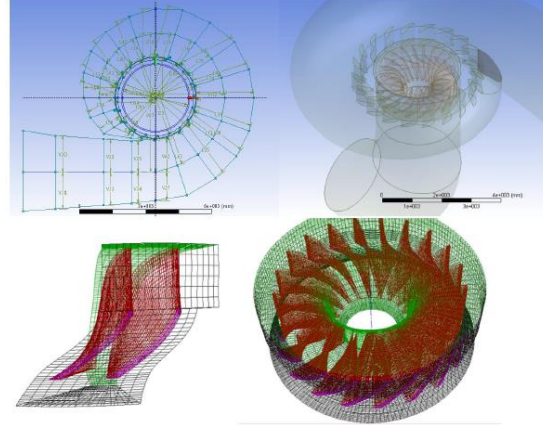
Fig. 1. Model geometries (Model geometrileri)

As a result of the calculation, 20 wicket gates were used in the turbine spiral case (Figure 2). The fixed number of wicket gates in the Figure is 20 and the modification to the wicket gate angles was made changing the "β_{ij}" angle from the "q" point. The rotor blade number was set to 17 (Model 1) and (Model 2) to analyze the principle of different denominators for the fixed blade number and the rotor blade number after drawing rotor blade profiles (Figure 3).
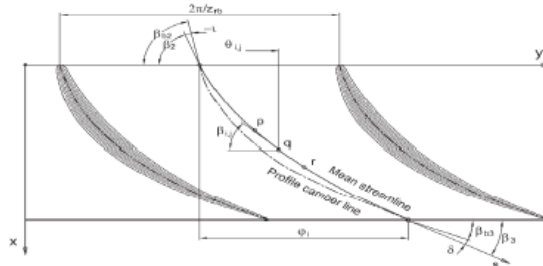
Fig. 2. Wicket gate profile (Yönlendirme kanat profili)
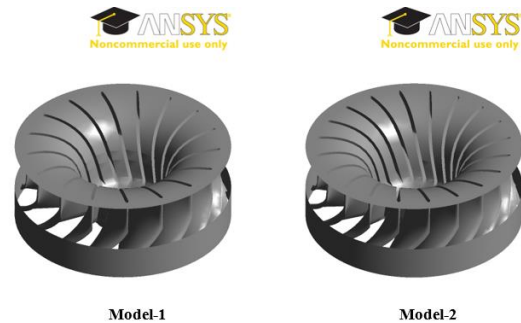
Fig. 3. Rotor views of Model and Model 2 (Model-1 ve Model-2'ye ait rotor görünümleri)

2.2. Meshing Process (Düğümleme İşlemleri)

The Meshing module, which is important to achieve the most accurate conclusion in the computational analysis of the geometric model, was established in 3D. Tetragonal, Wedge, and Pyrisma mesh structures were used in the 3D meshs in the meshing module. Considering quality of the meshs that are important for convergence in the computational solution, quality is known to increase with a skewness value closer to 0 and decrease with a skewness value closer to 1 [14,15,16]. Considering the skewness values of the meshs of two models in this study, close to 90% have a mesh quality below 0.5. These meshs have 750.456 nodes and 3.846.257 elements. The table graphic of mesh quality is provided in Figure 4.
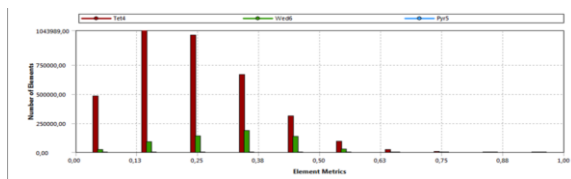
Fig. 4. Mesh quality (Düğüm kalitesi)

In the mesh module, the curvative method was used, high mesh quality was obtained, and mesh quality was increased by setting the span angle center between 12-36°. On the other hand, a five-layer inflation was configured to better see the boundary layer and flow regimes to occur in areas close to the boundary. The growth rate between these layers was kept as 1.2. Analyses are made in rotating systems by using the coordinate system. These systems are used by stating the boundaries on the reference axis in angular velocity or revolution number according to their respective axis. While analyzing the equations of motion depending on the rotating axis, it is required to enter the relative velocity or angular velocity for the rotating reference axis boundary. In this study, an angular velocity $26.16s^{-1}$ was entered for a -1 counterclockwise rotation on the y axis.

2.3. Numerical modelling of turbulent fluid flow (Türbülanslı Akşta Sayısal Model)

For a stable and three-dimensional flow, the conservation of mass is described by the following continuity equation:

$$\frac{\partial(\rho u)}{\partial x} + \frac{\partial(\rho v)}{\partial y} + \frac{\partial(\rho w)}{\partial z} = 0 \qquad (1)$$

Here, u, v, w represent the velocity values in x, y, z directions, respectively. For a stable and three-dimensional turbulent flow, equations of momentum are as follows;

$$\rho \frac{Du}{Dt} = \frac{\partial(-p+\tau_{xx})}{\partial x} + \frac{\partial \tau_{yx}}{\partial y} + \frac{\partial \tau_{zx}}{\partial z} + S_{Mx} \qquad (2)$$

$$\rho \frac{Dv}{Dt} = \frac{\partial \tau_{xy}}{\partial x} + \frac{\partial(-p+\tau_{yy})}{\partial y} + \frac{\partial \tau_{zy}}{\partial z} + S_{My} \qquad (3)$$

$$\rho \frac{Dw}{Dt} = \frac{\partial \tau_{xz}}{\partial x} + \frac{\partial \tau_{yz}}{\partial y} + \frac{\partial(-p+\tau_{zz})}{\partial z} + S_{Mz} \qquad (4)$$

In these equations, the surface stresses and body forces are described separately such that the contributions from body forces are designated as source terms, i. e., S_{Mx}, S_{My}, S_{Mz}. Note that, in a model, the body force originating from gravity is represented by source terms having values of $S_{Mx} = 0$, $S_{My} = -\rho g$, $S_{Mz} = 0$ [14,15]. When a incompressible fluid flows through a Francis turbine, the analysis of the flow for the entire system is performed by using the following forms of the continuity equation and Reynolds-averaged Navier – Stokes equation [14];

$$\rho \frac{Du}{Dt} = -\frac{\partial p}{\partial x} + div(\mu\, grad u) + S_{Mx} \qquad (5)$$

$$\rho \frac{Dv}{Dt} = -\frac{\partial p}{\partial y} + div(\mu\, grad v) + S_{My} \qquad (6)$$

$$\rho \frac{Dw}{Dt} = -\frac{\partial p}{\partial z} + div(\mu\, grad w) + S_{Mz} \qquad (7)$$

It is possible to write the Navier – Stokes equation in a more suitable form such that it can be used in the development of the finite volume method. Reynolds number is frequently used in the modeling of the turbulent flow and thereby the effects of turbulent flow are frequently given by Reynolds stresses, s_{ij}, which are calculated from the k-ε turbulence model. It should be noted that in order to convert the Reynolds-averaged Navier – Stokes equations to algebraic equations, unstructured finite volume approach is used in the code of the model and these algebraic equations are solved numerically [14,15].

2.3.1. Transport equations for the k- ε model (k-ε transport denklemi)

The transport equations given below are used to derive the turbulent kinetic energy and its rate of dissipation:

$$\frac{\partial}{\partial t}(\rho k) + \frac{\partial}{\partial x_i}(\rho k u_i) = \frac{\partial}{\partial x_j}\left[\left(\mu + \frac{\mu_t}{\sigma_k}\right)\frac{\partial k}{\partial x_j}\right] + G_k + G_b - \rho\varepsilon - Y_M + S_k \qquad (8)$$

$$\frac{\partial}{\partial t}(\rho\varepsilon) + \frac{\partial}{\partial x_i}(\rho\varepsilon u_i) = \frac{\partial}{\partial x_j}\left[\left(\mu + \frac{\mu_t}{\sigma_\varepsilon}\right)\frac{\partial\varepsilon}{\partial x_j}\right] + c_{1\varepsilon}\frac{\varepsilon}{k}(G_k + c_{3\varepsilon}G_b) - c_{2\varepsilon}\rho\frac{\varepsilon^2}{k} + S_\varepsilon \qquad (9)$$

2.3.2. Transport Equations for the RNG k-ε Model (k-ε RNG transport denklemi)

The RNG model has a similar form to the standard k- ε model

$$\frac{\partial}{\partial t}(\rho k) + \frac{\partial}{\partial x_i}(\rho k u_i) = \frac{\partial}{\partial x_j}\left[\left(\alpha_k \mu_{eff}\frac{\partial k}{\partial x_j}\right)\right] + G_k + G_b - \rho\varepsilon - Y_M + S_k \qquad (10)$$

$$\frac{\partial}{\partial t}(\rho\varepsilon) + \frac{\partial}{\partial x_i}(\rho\varepsilon u_i) = \frac{\partial}{\partial x_j}\left(\alpha_k \mu_{eff}\frac{\partial\varepsilon}{\partial x_j}\right) + C_{1\varepsilon}\frac{\varepsilon}{k}(G_k + C_{3\varepsilon}G_b) - c_{2\varepsilon}\rho\frac{\varepsilon^2}{k} - R_\varepsilon + S_\varepsilon \qquad (11)$$

Here, the turbulent kinetic energy as a result of the mean velocity gradient is given by G_k. Similarly, G_b describes the turbulent kinetic energy due to buoyancy. It should be noted that the mean velocity gradient and buoyancy

are calculated as depicted in the modelling turbulent production and effects of buoyancy on turbulence in the k-ε models, respectively. Y_M represents the contribution of the fluctuating dilatation incompressible turbulence to overall dissipation rate, calculated as described in effects of compressibility turbulence to the overall dissipation rate, calculated as described effects of compressibility on turbulence in the k-ε models. The quantities α_k and α_ε are inverse effective Prandtl number for k and ε, respectively. S_k and S_ε are user-defined source terms [14].

2.4. Boundary conditions (Sınır Şartları)

The system was modeled in three main parts according to the calculated values. Using the pressure-based analysis system, water at 23°C was used in the system, defined as the spiral case, rotating wheel, and outlet pipe. Creating a flow and control volume for the rotating wheel, the y rotating axis was defined by entering an angular velocity value of 250 min^{-1}. Moreover, the k-Ɛ model and "swirl dominated flow" were used in turbulent analyses for rotating systems and flows with a high Reynolds number. 13 bars of pressure for x=1 direction in cartesian coordinates was used as inlet pressure as an inlet boundary condition. Inlet length of run as well as turbulent viscosity values were defined as 10 %.

In the model, which was defined as "pressure outlet" at the outlet boundary condition, pressure and velocity values originating from adjacent surfaces were used.

2.5. Resolution Phase

When the dot products of pressure and viscous forces with a specific force vector, a, are summed up the total force component along that force vector is obtained. By this way, pressure and viscous force components of the total force in the direction of the vector a can be expressed separately:

$$F_a = \vec{a}.\vec{F_p} + \vec{a}.\vec{F_v} \qquad (12)$$

where a is specified force vector, F_p is pressure force vector, F_v is viscous force vector. Apart from pressure and viscosity based forces and total force, the corresponding force coefficients can be calculated for selected Wall zones by taking the reference values into consideration. Then, these force coefficients are divided by $\rho v^2/2$.

3. RESULTS AND DISCUSSION (BULGULAR VE TARTIŞMA)

Convergence curves were obtained from analyses of two models. Using the analyses, pressure, velocity, friction effects, moment, flow lines, and gradients, which are difficult to observe under normal conditions, were observed. Pressure and velocity values for points on the spiral case, fixed channel inlets and outlets and the outlet pipe in different models were reviewed.

3.1. Torque and Power Changes (Tork ve Güç Değişimleri)

Torque, output, and power factors were evaluated by changing wicket gate angles, which were positioned at

equal distances in the spiral case and allowed for conversion of the tangential velocity of the fluid to work in the most efficient way. Force and torque values can be directly measured from the fluent and CFD-Post module or can be obtained from the Euler moment equation. Force and torque values calculated separately for every model by the software are listed in Table 2. Values obtained by multiplying the torque values obtained after the analysis of the models in the software by angular velocities were provided as the turbine power.

Table 2. Torque and power for wicket gate angles (Yönlendirme kanat açısına göre Tork ve Güç değerleri)

Angle	Model 1		Model 2	
	Torque (x10^{6}Nm)	Turbine power (MW)	Torque (x10^{6}Nm)	Turbine power (MW)
12°	1.747	45.706	1.554	40.656
15°	1.834	47.986	1.725	45.128
18°	1.962	51.337	1.866	48.482
21°	2.032	53.175	1.933	50.589
23°	2.054	53.736	1.946	50.931
24°	2.068	54.122	1.968	51.500
25°	2.029	53.081	1.975	51.682
27°	2.032	53.162	1.951	51.059
30°	2.010	52.605	1.930	50.508
33°	1.960	51.274	1.879	49.165
36°	1.939	50.729	1.790	46.829
39°	1.863	48.762	1.748	45.749
42°	1.807	47.287	1.677	43.896
45°	1.705	44.624	1.608	42.068
48°	1.554	40.675	1.518	39.711

A maximum turbine power of 55.03 MW was obtained for the flow rate and selected head parameters in turbine measurement. Considering the theoretical power values for Model 1, turbine output in the best wicket gate angles was 98.3%. In Model 2, the turbine had 93.5% output after a change of 24 degrees in the angle.

Table 3 demonstrates that Model 1 was more efficient than Model 2. Significant differences were obtained between torque values caused by wicket gate angles between 12° and 48° on the rotor in the model of the turbine data calculated accordingly. Separately evaluating the models, output and power loss occurred between 30-33% in different wicket gates. The extent of the difference is presented in Table 3.

Table 3. Turbine output loss by models (Modellere göre türbin verim kayıpları)

Angle	Model 1 (24°-48°)		Model 2 (24°-48°)	
	Torque (10^6Nm)	Turbine power (MW)	Torque (10^6Nm)	Turbine power (MW)
Highest output (24°)	2.068	54.122	1.975	51.682
Lowest output (48°)	1.554	40.675	1.518	39.711
Output loss	33.05%		30.14%	

The highest torque value was obtained at 24° in Model 1 and Model 2, based on the available data. An average output difference of 5.86% was obtained between the torque and power values of Model 1 and Model 2. As described in the purpose of the study, it clearly demonstrated the output difference arising from the principle of applying a different denominator for the wicket gate number and the rotor blade number in literature.
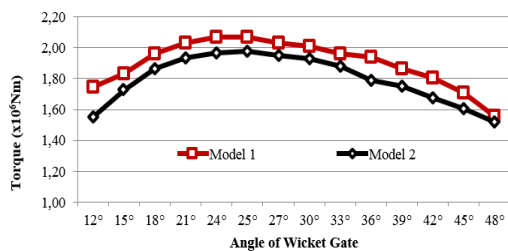
Fig. 4. Torque values of the models by the wicket gate angle (Yönlendirme kanat açısına göre modellerin tork değerleri)

A graphic is provided in Figure 4 for torque values obtained from the turbine rotor. A difference of 2×10^5Nm was observed as the average torque value between the models. The ratio between torque values and power values obtained from the fluent model equals to the radius of the turbine rotor.

It is clear that torque values obtained from the turbine rotor were higher between 18°-33°. The main reason is that the tangential velocity of the fluid discharged from the turbine wicket gates changes and the ratio of rotor input velocity (u) to rotor output velocity (v_1) differed by 0.5. The change in the power value that can be obtained from the turbine shaft for the number of revolutions known to be 26.16rad/s (250 min^{-1}) of the turbine with the torque values depending on the wicket gate angle is provided in Figure 5. The change between torque and turbine power was parallel. Maximum turbine power was obtained at a 24° blade angle for Model 1 and Model 2.
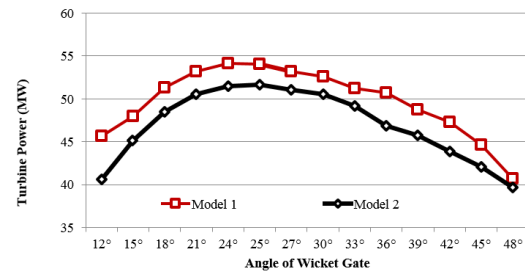
Fig. 5. Turbine power values by the wicket gate angle (Yönlendirme kanat açısına göre Türbin gücü değerleri)

For Model 2, the change in hydraulic output and rotor output by the wicket gate angle is provided in Figure 6. Maximum hydraulic and rotor output obtained from the velocity at the rotor inlet was obtained at the 24° wicket gate angle.
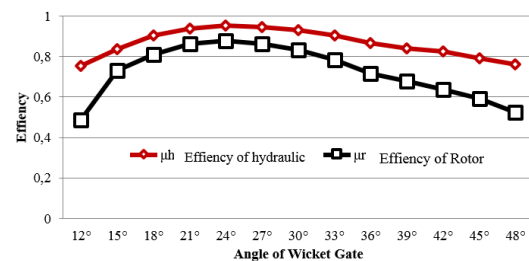
Fig. 6. Change in hydraulic and rotor outputs in the model by the wicket gate angle (Model-2 hidrolik ve rotor verimlerinim yönlendirici kanat açısı ile değişimi)

Power changes in the turbine rotor are provided in Figure 7. As seen in Figure 7a, power required for rotation gradually decreased from the center of the turbine rotor towards the blade inlets. At this point, the necessary power for a rotation speed of 250min^{-1} of the rotor varies by the turbine rotor radius.
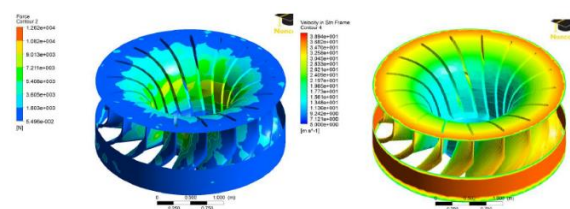
Fig. 7. Power on turbine rotor surfaces 7-a, velocity values 7b, (7a Türbin rotor yüzeylerinde oluşan kuvvet, 7-b hız değerleri)

The general condition of velocity distribution in the turbine rotor is provided in Figure 7b. Uniform velocity distribution on the shaped rotor explains how pressure forces transferred to the rotor are absorbed. Velocity decreases by about ½, considering velocity distributions at the rotor inlet and the rotor outlet. This provides a value that is very close to maximum turbine outputs.

3.2. Velocity and Pressure Changes (Hız ve Basınç Değişimleri)

The selection of points on the turbine is generally based on geometric model sections and closeness to the center (Figure 8). Using the CFD-Post module, pressure and velocity values for all angle changes in Model 1 and Model 2 were obtained from the coordinates of the concerned points.
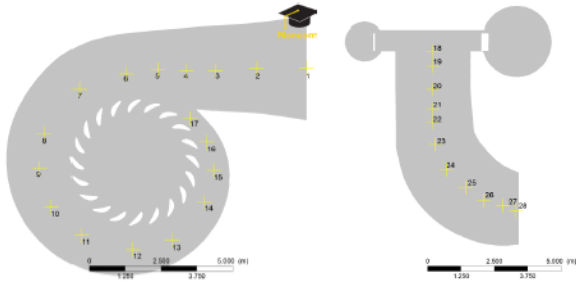
Fig. 8. Points selected on the spiral case (Salyangoz üzerinde seçilen noktaların gösterimi)

3.2.1 Velocity Changes (Hız Değişimleri)

This section evaluates velocity distributions on the system for the turbine rotor with 17 blades within point, plane, and flow volumes. Figure 9 displays values on the points determined for the three models with the highest output in the concerned velocity distribution.
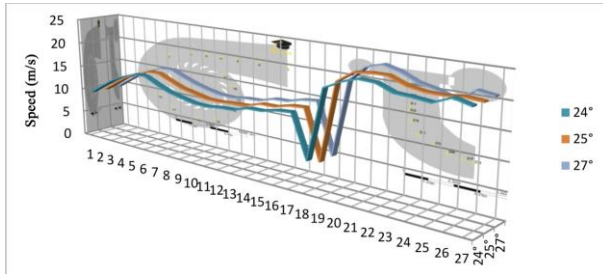
Fig. 9. Turbine point velocity graphic for Model 1(Model-1 için türbin noktasal hız grafiği)

The role of the spiral case is to ensure that the supply water enters at equal velocities and equal pressures around the rotor blades. Velocity distributions along the spiral case in the turbine decreased starting from the entry point of the fluid into the rotor (from point 4 to point 17) and exhibited a velocity change of 3m/s. Velocity significantly decreased in the dead core zone where the fluid hits the turbine rotor and is directed to the outlet pipe. Acceleration gradually increased after this point, starting from the inlet of the outlet pipe. After the outlet pipe, velocity decreased due to vortex flows and was directed to the diffuser from the outlet pipe.

The results of the velocity analyses in Model 1 and Model 2 were examined. Changes are clearly displayed with comparisons between the same wicket gate numbers and velocity limits in the two models. The point values are provided in graphics. Moreover, statements about similar changes in the two models are explained further and supported with images.
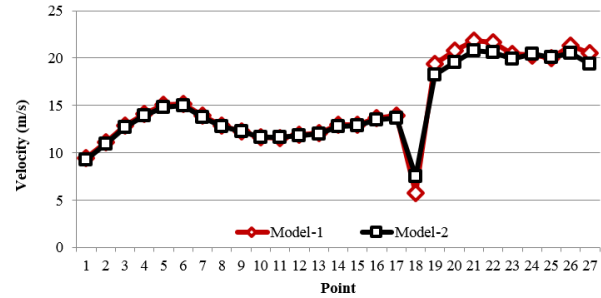
Fig. 10. Velocity changes in Model 1 and Model 2 (Model-1 ve Model-2 hız değişimleri)

Comparison between two models for the highest output level at 24° is provided in Figure 10. Velocity distributions in the spiral case section in the figure have similar values. In addition, there was a difference in velocity distribution for points 17 and 18 where inlet-outlet velocity values were provided as used in the torque-power calculation. The main parameter that caused Model 1 to be more efficient compared to Model 2 was mainly obtained from this change. In Model 1, the pressure of the fluid received by the rotor was absorbed and velocity in the dead core zone dropped by approximately 3 m/s compared to Model 2. The main reason for the 5% increase in turbine output in Model 1 can be concluded to arise from this change in velocity at the rotor outlet.

Figure 11 displays changing velocity flows throughout the turbine system. Velocity distribution at the outlet pipe and flow lines show differences in terms of value and number between two models. The vortex flows, described for their effects and significance, can be clearly seen to condense along the outlet pipe in Model 2. It can be concluded that the viscous forces of these vortexes increase, and thus, changes in velocity at rotor inlets-outlets directly decrease the torque value. The decrease in torque values was 5% as shown in Table 5.3.
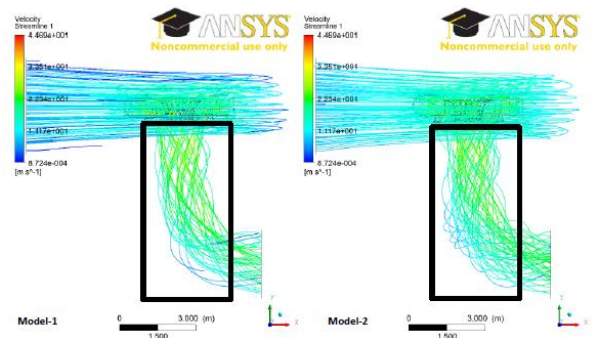
Fig. 11. Model 1 and Model 2 velocity flow lines (24° angle) (Model-1 ve Model-2 hız akım çizgileri)

In conclusion, velocity fluctuations throughout turbine systems, depending on changes in blade numbers and guide angles preferred in turbines, directly affect turbine output. Another important point other than torque and output is vibrations in the turbine shaft due to fluctuations in the outlet pipe. Every vortex to be formed for additional blades causes more yaw and vibration in the turbine shaft and directly affects turbine life. Vortex flows occur depending on the turbine specific velocity in the dead water core, as shown in Figure 12. They support the formation of turbulent flow areas that cannot be calculated by the intensity of vortex flows. The directions of the dead water core and vortex flows at a 24° angle, depending on changing velocities in the outlet pipe section, are provided in Figure 12.
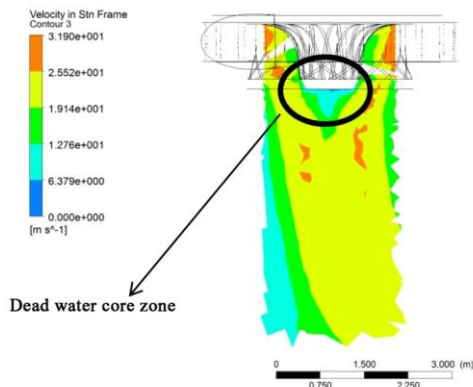
Fig. 12. Water core zone in the outlet pipe section (24° angle) (Çıkış borusu kesitinde oluşan ölü su çekirdek bölgesi (24°'lik açı için))

In this figure, water velocity in the dead water core zone is very low. There are flows at the edges of the core zone due to rotor rotation. Velocity distribution in the outlet pipe is clearly seen in the rectangle section view. Vortex developments in the outlet pipe in Model 1 are provided in Figure 13. Although the flow lines emerging after the dead core zone between 12°-18° have very low velocity values, the number of rotating flows is high. The vortex effects, which begin to occur at the start of the outlet pipe after a change of 36°, are lower between 36°-48° compared to Model 2.
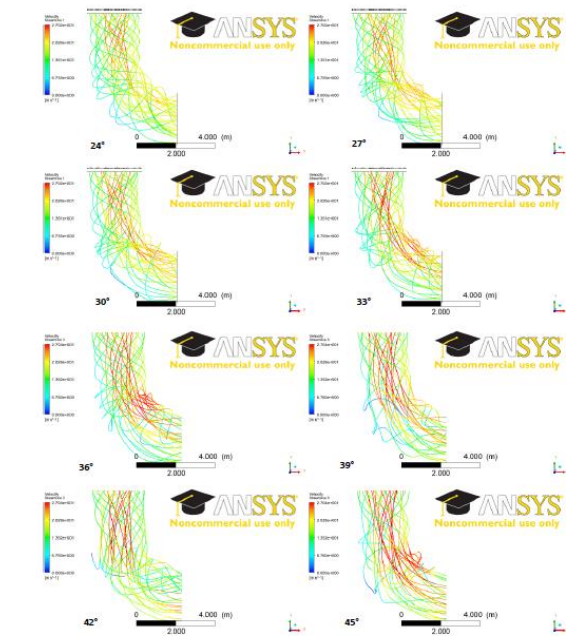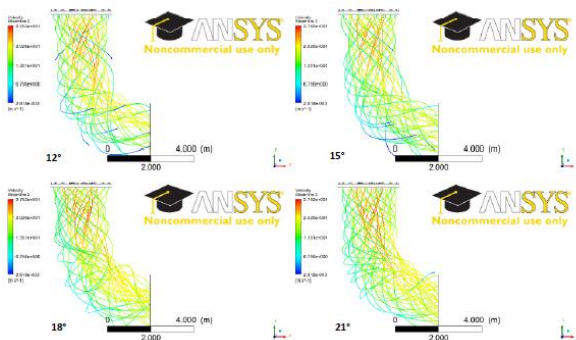
Fig. 13. Development of flow lines in 12-45° outlet pipe (12-45° çıkış borusunda oluşan akım çizgilerinin gelişimi)

3.2.2. Pressure changes (Basınç Değişimleri)

According to the results of the analysis in the models, pressure change in the highest output in the spiral case section had homogenous development. It is clearly observed that high pressure water is absorbed in the area of the turbine rotor and energy is transferred to the turbine rotor. Turbine power absorption seems problem free at this point.
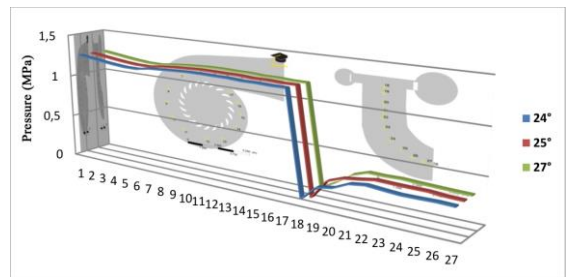
Fig. 14. Pressure change in the turbine spiral case and outlet pipe (Türbin salyangozu ve çıkış borusundaki basınç değişimi)

Figure 14 provides a pressure change graphic for Model 1 at 24°-25°-27°, with high efficiency wicket gates. Thirteen bar pressure, defined to be the requirement for input along the spiral case section in the graphic for changing pressure throughout the turbine, remained almost fixed homogenously along the entire spiral case. High pressure water entering from the turbine spiral case was absorbed by the turbine rotor and was transferred to the turbine shaft between points 17 and 18. A pressure change of approximately 11 bars occurred in the turbine. Low pressure water was discharged from the outlet pipe

with the effect of gravity and density (Figure 14). Pressure distribution in the outlet pipe is provided in Figures 15 and 16. Pressure distribution according to the spiral case section seems to increase in areas closer to the outlet pipe.
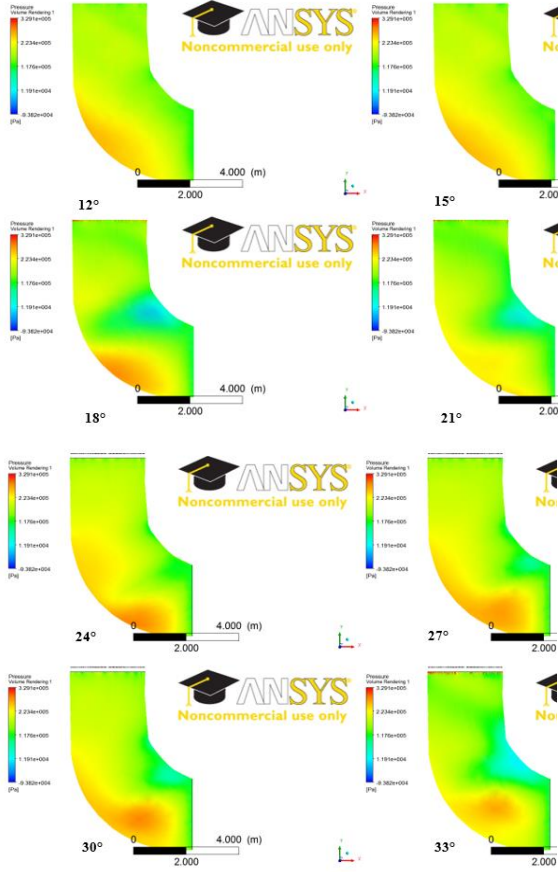
Fig. 15. Pressure distribution in the outlet pipe between 12°-33° (12°-33° aralığında çıkış borusunda ortaya çıkan basınç dağılımı)
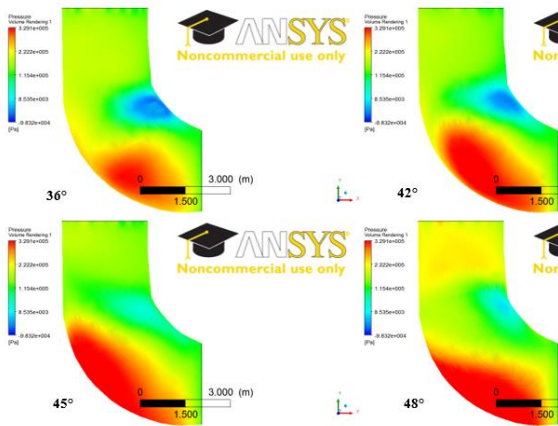
Fig. 16. Pressure distribution in the outlet pipe between 36°-48° (36°-48° aralığında çıkış borusunda ortaya çıkan basınç dağılımı)

Pressure distribution in the outlet pipe depending on varying angles is clearly provided in Figures 15 and 16. Certain areas were not homogenous and pressure increases emerged, particularly in areas closer to the end of the outlet pipe in the angle variance range of 36°-48°. While pressure reached 4 bars on the bottom of the outlet pipe at 36°-48°, it exhibited a vacuum effect in the upper area. This caused the system to create a turbulent flow, and generate pressure fluctuations, knocking, and noise and thus, vibration in the turbine shaft.

4. CONCLUSION (SONUÇLAR)

It is difficult to design and calculate many components due to complex structures, considering operating conditions of turbines. The two phase analysis method used in the study reviewed changes in torque, output, and resistance of turbine efficiencies with blade angles. The output difference by angles in turbine efficiencies varied between 5-14%.

Computational fluid dynamics software proved useful in determining flow lines around the turbine spiral case and blades and observing the effect of tangential velocity components on the turbine rotor. Furthermore, changes in blade angles and changes in force and torque values in the turbine rotor were clearly observed. For the efficient range of 24°-27° for Model 1 and Model 2, obtaining same results in different studies in the field [7] is very important for accuracy of this study.

Pressure distribution was homogenous for boundary conditions, which were determined at the inlet along the spiral case, and provided operating pressure in the models. The two-phased model comparisons in the turbine rotor described the effects of reduced number of blades and different number of blades and wicket gates. The outlet pipe analyses in Model 1 and Model 2 examined flow fluctuations and vortex formations. The number and intensity of the vortexes as well as vibrations they would cause in Model 1 were low.

Output differences between the two models demonstrated the effect of pressure absorption and velocity changes in the turbine rotor. The fact that results from the models generated similar values indicated the accuracy of the analysis results. Benefiting from CFD and FEM software before production in turbine design can be said to offer important advantages in terms of time, cost, and reliability.

REFERENCES (KAYNAKLAR)

1. Čarija Z, Z. Mrša, Complete Francis turbine flow simulation for the whole range of discharges. *In: 4th International Congress of Croatian Society of Mechanics*, Bizovac, Croatia, 105–110,(2003).
2. Ruofu X, Zhengwei W., Yongyao L., "Dynamic Stresses in A Francis Turbine Runner Based On Fluid-Structure Interaction Analysis", *Tsinghua Sci Technology*,13(5): 587–592, (2008).
3. Choi H. J., Mohammed A.Z., Hyoung-Woon R., Pil-Su H., Sueg-Young O., Young-Ho L., "CFD Validation of

Performance Improvement of a 500 kW Francis Turbine", *Renewable Energy*, 54: 111-123, (2003).

4. Saaed, R.A., Galybin A.N., Popov V., "Modelling of flow-induced stresses in a Francis turbine runner*", Advances in Engineering Software*, 41: 1245–1255,(2010).

5. Okyay, G., Çelebioğlu K., Aydın İ., Ger A.M., "Design of a Francis Type Water Turbine Using Computational Fluid Dynamics Methods", *Nuclear & Renewable Energy Resources Conference With International Participation*, Ankara-Turkey, 388-394, (2009).

6. Chen, W.C., K. Celebioglu, "Structural Analysis of Francis Type Turbine using Finite Element Method*", In: Nuclear & Renewable Energy Resources Conf. with Int. Particip*., Ankara-Turkey, 378-383, (2009).

7. Jain S., Saini R. P., Kumar A., "CFD Approach for Prediction of Efficiency of Francis Turbine", *IGHEM, AHEC*, IIT, Roorkee, India, (2010).

8. Pennacchi P., Chatterton S., Bachschmid N., Pesatori E., Turozzi G., "A Model to Study the Reduction of Turbine Blade Vibration Using The Snubbing Mechanism", *Mechanical Systems and Signal Processing*, 25: 1260–1275, (2011).

9. Zhanga H., L. Zhang, "Numerical Simulation of Cavitating Turbulent Flow in a High Head Francis Turbine at Part Load Operation with Openfoam", *International Conference on Advances in Computational Modeling and Simulation*, Procedia Engineering 31: 156–165, (2012).

10. Bing B. B., Zhang L., Guo T., Liu C. Analysis of Dynamic Characteristics of the Main Shaft System in a Hydro-turbine Based on ANSYS, *Procedia Engineering*, 31:654 – 658, (2012).

11. Nilsson H., Davidson L. A., "Numerical Comparison of Four Operating Conditions in a Kaplan Water Turbine", *Focusing on Tip Clearance Flow Published in the proceedings of the 20th IAHR Symposium*,Charlotte, North Carolina, U.S.A. http://www.hcipub.com/iahr2000

12. Başeşme H., *Hydroelectric Power Plants*, General Directorate of EUAS, Ankara, 15-95, (2003).

13. Cengel Y., Cimbala J.M., *Fluid Mechanics: Fundamentals and Applications*, Ed. 3, McGraw-Hill, New York, USA,(2014).

14. ANSYS Inc., *Fluent Theory Guide*, Southpointe Technology Drive Canonsburg, USA,(2011).

15. Versteeg H.K., Malalasekera W., *An Introduction to Computational Fluid Dynamics The Finite Volume Method*, Pearson Prentice Hall Second edition, 1-16.,(2007).

16. Sözen A., Keçel, S., Yavuzcan H.G., "The Effect of the Angle of The Wicket Gate on Turbine Efficiency And Strength in Francis Type Turbines", *Journal of Gazi University Engineering and Architecture Faculty*, 29(2):243-252, (2014).